Towards Predictable Precision Manipulation of Unknown Objects with Underactuated Fingers

Raymond R. Ma, Nicolas Rojas and Aaron M. Dollar

Abstract This paper describes a new concept in underactuated hand design, motivated by a study of parallel mechanisms. Inspired by the end-effector motion and system reconfiguration in parallel wrists, we propose a morphology of fingers such that during fingertip precision manipulation the instantaneous screw axes, which describe the displacement of the grasped object respect to the palm of the hand, always intersect at the same known fixed point regardless of the object's particularities. A physical hand was built to evaluate the feasibility of the design concept in improving precision manipulation capabilities while preserving power-grasping functionality. The tendon-driven hand is underactuated, with one actuator for each of the two-degree-of-freedom fingers, and passive rotary fingertips are used to minimize slip at contact points during manipulation. Experimental results with the hand demonstrate the effectiveness of the concept, thus encouraging further research in the area.

Keywords Underactuated hands · Precision manipulation · Kinematic analysis

1 Introduction

The ability to use the fingers to manipulate a grasped object held within the fingertips, often called "precision manipulation," is an important functionality extending the utility of robotic hands beyond simply acquiring and holding objects

R.R. Ma (✉) · N. Rojas
Yale University, 9 Hillhouse Ave, New Haven, CT 06511, USA
e-mail: raymond.ma@yale.edu

N. Rojas
e-mail: nicolas.rojas@yale.edu

A.M. Dollar
Yale University, 15 Prospect St, New Haven, CT 06520, USA
e-mail: aaron.dollar@yale.edu

X. Ding et al. (eds.), *Advances in Reconfigurable Mechanisms and Robots II*,
Mechanisms and Machine Science 36, DOI 10.1007/978-3-319-23327-7_79

(i.e. grasping) [1]. Such motions are useful for making fine adjustments to the position and orientation of grasped objects and negotiating singularities/joint limits and environmental obstacles, among others [2]. However, precision manipulation is challenging, in part because the hand/object configuration is typically over-constrained and requires redundant control schemes to address [3]. This is further complicated in the common situation where the precise object geometry and/or fingertip contact locations are not known, making the execution of manipulation movements extremely difficult. Our past work [4] suggests that underactuation assists in passively maintaining stable precision grasps through reconfiguration and the use of elastic elements. However, manipulation capabilities needed to be manually sampled and evaluated for each distinct object geometry, and slip at contact was a prevalent issue. In this paper, we examine a hand topology in which the joint axes of the fingers always intersect at the same point and thereby simplifying the manipulation planning problem.

Although mechanical design of robotic hands has largely focused on the performance of individual fingers [5, 6], several researchers have modeled multi-fingered manipulation as a closed-chain system involving the hand and the grasped object [7, 8], and others have established frameworks to describe dexterous in-hand manipulation in the context of parallel mechanisms [9–11]. As long as the contact conditions remain valid, the closed-kinematic-chain model may be applied to the hand-object system, providing insight into the workspace of the system.

Inspired by the end-effector motion in parallel wrists [12, 13], we propose the design of a three-finger hand design, shown in Fig. 1, with two curved underactuated fingers and an opposable underactuated thumb, each with specialized rotary fingertips that minimize slip during manipulation. This hand design can move the object within the hand workspace about a fixed reference point, regardless of the object geometry or initial points of contact. The instantaneous screw axes, which describe the displacement of the grasped object respect to the palm of the hand, always intersect at the same known fixed point and correspond to a spherical motion. These design changes preserve the adaptive, power-grasping capability of underactuated fingers and can be applied to the base structure of commercial three-fingered hands, including the BarrettHand [14], Robotiq's three-finger gripper [15], and the iHY hand [16]. One of the fingers, denoted as the "thumb," has a static base, while the other two fingers can adduct/abduct in a coupled manner.

2 Spherical Motion During Precision Manipulation

A technique to characterize the precision manipulation capabilities of a given robot hand regardless of the particularities of the grasped object was presented in [9]. The approach extends the work of Hervé [17] and is based on a reduction of the graph of kinematic constraints related to the hand-object system through proper manipulations of the continuous subgroups of displacements generated by the hand joints and contacts. In this section we show that the finite displacement of the corresponding

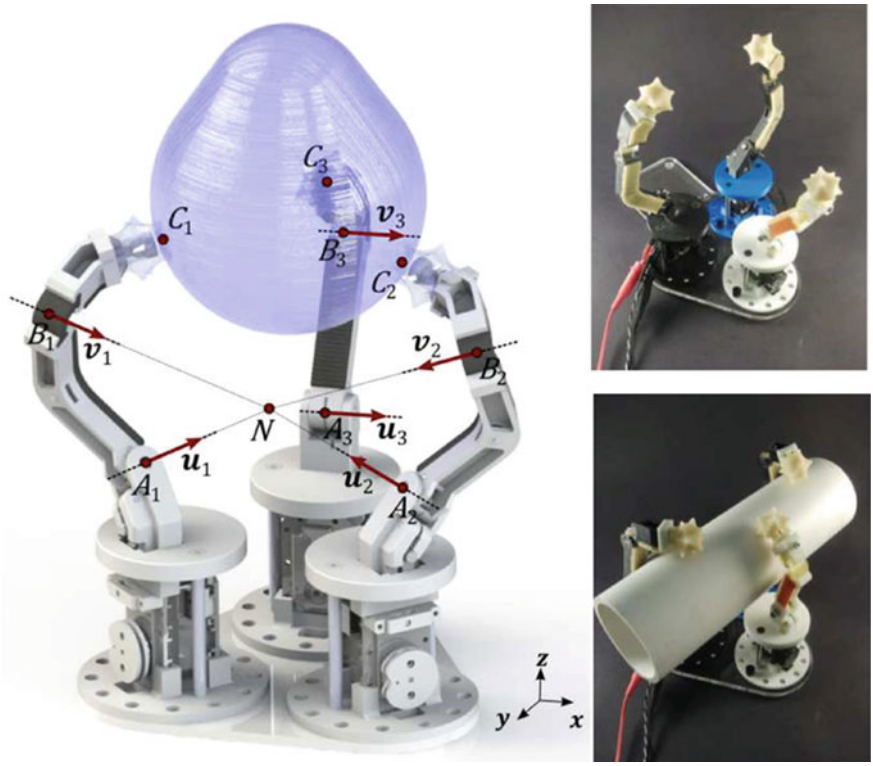

Fig. 1 The proposed hand with modified curved fingers and rotary fingertips designed for improving the precision manipulation capability of underactuated robot hands while preserving their power-grasping functionality

grasped object always reduces to a rotation around some axis passing through a fixed point. Such a point is in fact known from the geometry of the hand alone and corresponds to the intersection of the revolute axes of the curved fingers.

2.1 Precision Manipulation Analysis

Figure 1 shows the hand performing a precision grasp on a general object. During these tasks, the hand-object system is equivalent to a closed kinematic chain composed of eight links with three revolute-revolute-spherical serial limbs that connect the palm of the robot hand, or base, to the grasped object. The mobility of such closed kinematic chain (8 links, 9 joints in $\mathbb{R}^3$ with a total of 15 dof) is, applying the Hunt's form of the Chebychev–Grübler–Kutzbach criterion [3, 18].

According to the notation of Fig. 1, consider finger 1, one of the curved fingers, with contact point C_1. The axis of the proximal revolute joint is determined by a

unit vector $\boldsymbol{u}_1$ and any point, A_1, that belongs to the line defined by the rotational axis. Thus, point A_1 can be N, the point where the rotational axes of the curved fingers intersect. This kinematic pair corresponds to a kinematic constraint that forms the subgroup of displacements $\{\mathbf{R}(A_1, \boldsymbol{u}_1)\} = \{\mathbf{R}(N, \boldsymbol{u}_1)\}$, which restricts the movement between this proximal link and the palm. Similarly, for the finger 1's distal joint, the generated subgroup is $\{\mathbf{R}(B_1, \boldsymbol{v}_1)\} = \{\mathbf{R}(N, \boldsymbol{v}_1)\}$. For the case of the motion constraint between the fingertip and the object, the generated subgroup is $\{\mathbf{S}(C_1)\}$, a spherical rotation about point C_1. This contact model is kinematically equivalent to point contact with friction [19].

The above analysis is replicated for finger 2, the other curved finger. In the case of finger 3, the thumb, the axis of the proximal revolute joint, defined by the unit vector $\boldsymbol{u}_3$ and the point A_3, is parallel to the x-axis, as is the distal revolute joint. The resulting graph of kinematic constraints for the complete hand-object system is depicted in Fig. 2a. This graph is composed of eight nodes and nine edges, related to number of links and joints of the associated kinematic chain, respectively.

In order to obtain a reduced mathematical characterization of the displacement manifold of the grasped object relative to the palm of the proposed hand, we firstly apply, according to the notation of Fig. 2a, a serial reduction to the nodes 1, 2, 3, and 6. Then, we get

$$\mathcal{S}_1 = \{\mathbf{R}(N, \boldsymbol{u}_1)\} \cdot \{\mathbf{R}(N, \boldsymbol{v}_1)\} \cdot \{\mathbf{S}(C_1)\}. \tag{1}$$

Using the property of closure of groups, it can be easily proven that $\{\mathbf{S}(O)\} = \{\mathbf{R}(O, \boldsymbol{i})\} \cdot \{\mathbf{R}(O, \boldsymbol{j})\} \cdot \{\mathbf{R}(O, \boldsymbol{k})\}$, provided that $\boldsymbol{i}$, $\boldsymbol{j}$, and $\boldsymbol{k}$ are linearly independent vectors [20]. Let $\widehat{\boldsymbol{nc}}_1$ a unit vector that is parallel to the line defined by points N and C_1, and $\boldsymbol{j}_1$ and $\boldsymbol{k}_1$, two unit vectors that are linearly independent to it. Then,

$$\begin{aligned} \{\mathbf{S}(C_1)\} &= \{\mathbf{R}(C_1, \widehat{\boldsymbol{nc}}_1)\} \cdot \{\mathbf{R}(C_1, \boldsymbol{j}_1)\} \cdot \{\mathbf{R}(C_1, \boldsymbol{k}_1)\} \\ &= \{\mathbf{R}(N, \widehat{\boldsymbol{nc}}_1)\} \cdot \{\mathbf{R}(C_1, \boldsymbol{j}_1)\} \cdot \{\mathbf{R}(C_1, \boldsymbol{k}_1)\}, \end{aligned} \tag{2}$$

since $\{\mathbf{R}(C_1, \widehat{\boldsymbol{nc}}_1)\} = \{\mathbf{R}(N, \widehat{\boldsymbol{nc}}_1)\}$. Substituting (2) into (1), we have

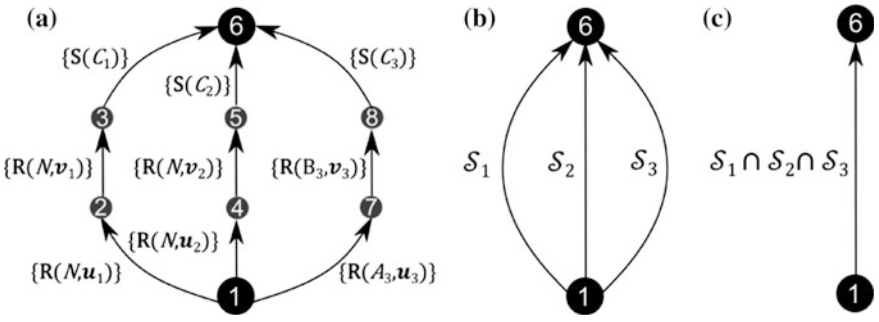

Fig. 2 The graph of kinematic constraints of the hand-object system for the spherical hand (**a**) and its corresponding reduction (**b**, **c**)

$$\mathcal{S}_1 = \{\mathbf{S}(N)\} \cdot \{\mathbf{S}(C_1)\}, \tag{3}$$

Applying the same reduction to the nodes 1, 4, 5, and 6, we get

$$\mathcal{S}_2 = \{\mathbf{S}(N)\} \cdot \{\mathbf{S}(C_2)\}. \tag{4}$$

For the case of the set of nodes 1, 6, 7, and 8 we have (with $\boldsymbol{u}_3 \parallel \boldsymbol{v}_3 \parallel \boldsymbol{x}$)

$$\mathcal{S}_3 = \{\mathbf{R}(A_3, \boldsymbol{u}_3)\} \cdot \{\mathbf{R}(B_3, \boldsymbol{v}_3)\} \cdot \{\mathbf{S}(C_3)\} = \{\mathbf{R}(A_3, \boldsymbol{x})\} \cdot \{\mathbf{R}(B_3, \boldsymbol{x})\} \cdot \{\mathbf{S}(C_3)\}. \tag{5}$$

Since the subgroup $\{\mathbf{R}(C_3, \boldsymbol{x})\}$ is a proper subset of the subgroup $\{\mathbf{S}(C_3)\}$, that is, $\{\mathbf{R}(C_3, \boldsymbol{x})\} \subset \{\mathbf{S}(C_3)\}$, then, by the property of closure in groups, we get $\{\mathbf{R}(C_3, \boldsymbol{x})\} \cdot \{\mathbf{S}(C_3)\} = \{\mathbf{S}(C_3)\} (\forall x, x \in \{\mathbf{R}(C_3, \boldsymbol{x})\} \cdot \{\mathbf{S}(C_3)\}, x \in \{\mathbf{S}(C_3)\})$. Hence,

$$\begin{aligned} \mathcal{S}_3 &= \{\mathbf{R}(A_3, \boldsymbol{x})\} \cdot \{\mathbf{R}(B_3, \boldsymbol{x})\} \cdot \{\mathbf{R}(C_3, \boldsymbol{x})\} \cdot \{\mathbf{S}(C_3)\} \\ &= \{\mathbf{G}(\boldsymbol{x})\} \cdot \{\mathbf{S}(C_3)\}, \end{aligned} \tag{6}$$

where $\{\mathbf{G}(\boldsymbol{u})\} = \{\mathbf{R}(O, \boldsymbol{u})\} \cdot \{\mathbf{R}(P, \boldsymbol{u})\} \cdot \{\mathbf{R}(Q, \boldsymbol{u})\}$, with $O \neq P \neq Q$, corresponds to the subgroup of planar gliding motions determined by the unit normal vector $\boldsymbol{u}$. These three serial operations reduce the original graph of kinematic constraints to a graph of two nodes with three edges as shown in Fig. 2b.

We next apply parallel reduction to simplify the three kinematic constraints to a single couple of edges. The intersection ($\cap$) of two kinematic constraints is basically the intersection as in set theory. For instance, the intersection between a spherical rotation $\{\mathbf{S}(N)\}$ and a planar gliding motion $\{\mathbf{G}(\boldsymbol{u})\}$ is $\{\mathbf{R}(N, \boldsymbol{u})\}$. Similarly, $\{\mathbf{S}(O)\} \cap \{\mathbf{S}(P)\} = \{\mathbf{R}(O, \widehat{\boldsymbol{op}})\} = \{\mathbf{R}(P, \widehat{\boldsymbol{op}})\}$ with $\widehat{\boldsymbol{op}} = \overrightarrow{OP} / \overrightarrow{OP}$.

For the case of the kinematic constraints $\mathcal{S}_1$ and $\mathcal{S}_2$, we have

$$\begin{aligned} \mathcal{P}_1 &= \mathcal{S}_1 \cap \mathcal{S}_2 \\ &= \{\mathbf{S}(N)\} \cdot \{\mathbf{S}(C_1)\} \cap \{\mathbf{S}(N)\} \cdot \{\mathbf{S}(C_2)\} \\ &= \{\mathbf{S}(N)\} \cdot (\{\mathbf{S}(C_1)\} \cap \{\mathbf{S}(C_2)\}) \\ &= \{\mathbf{S}(N)\} \cdot \{\mathbf{R}(C_1, \widehat{\boldsymbol{c}_1\boldsymbol{c}_2})\}. \end{aligned} \tag{7}$$

For $\mathcal{S}_2$ and $\mathcal{S}_3$, we get

$$\begin{aligned} \mathcal{P}_2 &= \mathcal{S}_2 \cap \mathcal{S}_3 \\ &= \{\mathbf{S}(N)\} \cdot \{\mathbf{S}(C_2)\} \cap \{\mathbf{G}(\boldsymbol{x})\} \cdot \{\mathbf{S}(C_3)\} \\ &= \{\mathbf{R}(N, \boldsymbol{x})\} \cdot \{\mathbf{R}(N, \widehat{\boldsymbol{n}\boldsymbol{c}_3})\} \cdot \{\mathbf{R}(C_2, \boldsymbol{x})\} \cdot \{\mathbf{R}(C_2, \widehat{\boldsymbol{c}_2\boldsymbol{c}_3})\} \\ &= \{\mathbf{R}(N, \boldsymbol{x})\} \cdot \{\mathbf{R}(N, \widehat{\boldsymbol{n}\boldsymbol{c}_3})\} \cdot \{\mathbf{S}_2(C_2)\}. \end{aligned} \tag{8}$$

where $\{\mathbf{S}_2(O)\} = \{\mathbf{R}(O,\boldsymbol{u})\} \cdot \{\mathbf{R}(O,\boldsymbol{v})\}$ is the submanifold included in $\{\mathbf{S}(O)\}$ defined as the composition of two different subgroups of rotations whose axes meet at a single point [21, 22]. Now, let $\widehat{\boldsymbol{nc}_2}$ a unit vector that is parallel to the line defined by points N and C_2, and $\boldsymbol{j}_2$ a unit vector that is linearly independent to it. Then, likewise as in the case of Eq. (2), we have

$$\{\mathbf{S}_2(C_2)\} = \{\mathbf{R}(N,\widehat{\boldsymbol{nc}}_2)\} \cdot \{\mathbf{R}(C_2,\boldsymbol{j}_2)\}. \tag{9}$$

Replacing (11) into (8), we get

$$\begin{aligned} \mathcal{P}_2 &= \{\mathbf{R}(N,\boldsymbol{x})\} \cdot \{\mathbf{R}(N,\widehat{\boldsymbol{nc}_3})\} \cdot \{\mathbf{R}(N,\widehat{\boldsymbol{nc}_2})\} \cdot \{\mathbf{R}(C_2,\boldsymbol{j}_2)\} \\ &= \{\mathbf{S}(N)\} \cdot \{\mathbf{R}(C_2,\boldsymbol{j}_2)\}, \end{aligned} \tag{10}$$

provided that $\boldsymbol{x}$, $\widehat{\boldsymbol{nc}_3}$, and $\widehat{\boldsymbol{nc}_2}$ are linearly independent vectors. Note that Eqs. (7) and (10) correspond to a 4-manifold, as it is required by the closed kinematic chain associated to the kinematic constraints $\mathcal{S}_1$ and $\mathcal{S}_2$, and $\mathcal{S}_2$ and $\mathcal{S}_3$, respectively.

After the application of the two presented parallel reductions, a graph of kinematic constraints of two nodes with two edges is obtained. The final operation to get the subset of displacements of the grasped object is a last parallel reduction applied to the constraints $\mathcal{P}_1$ and $\mathcal{P}_2$, shown in Fig. 2c. Thus, we have

$$\begin{aligned} \mathcal{P}_3 &= \mathcal{P}_1 \cap \mathcal{P}_2 \\ &= \{\mathbf{S}(N)\} \cdot \{\mathbf{R}(C_1,\widehat{\boldsymbol{c}_1\boldsymbol{c}_2})\} \cap \{\mathbf{S}(N)\} \cdot \{\mathbf{R}(C_2,\boldsymbol{j}_2)\} \\ &= \{\mathbf{S}(N)\} \cdot (\{\mathbf{R}(C_1,\widehat{\boldsymbol{c}_1\boldsymbol{c}_2})\} \cap \{\mathbf{R}(C_2,\boldsymbol{j}_2)\}) \\ &= \{\mathbf{S}(N)\}, \end{aligned} \tag{11}$$

where $\{\mathbf{R}(C_1,\widehat{\boldsymbol{c}_1\boldsymbol{c}_2})\} \cap \{\mathbf{R}(C_2,\boldsymbol{j}_2)\} = \{\mathbf{I}\}$, the identity displacement.

Equation (11) implies that the movement of a grasped object by this hand corresponds in general to a spherical rotation about N, the intersection point of the revolute axes of the curved fingers. This finite spherical motion is a 3-manifold, as it is required by the mobility of the associated kinematic chain of the hand-object system.

3 Mechanical Design

The fingers are based on designs from the Yale OpenHand Project [23], fabricated via Hybrid Deposition Manufacturing (HDM) [24], which combines 3D-printed body components and sacrificial mold features with traditional resin-casting techniques. Each two-link, underactuated finger is actuated by a single agonist tendon. The proximal joint is a revolute pin joint with a torsional return spring, and the distal joint produces similar behavior with a cast urethane, flexural joint made of material PMC-780 [25]. The flexure joint has limited out-of-plane compliance to

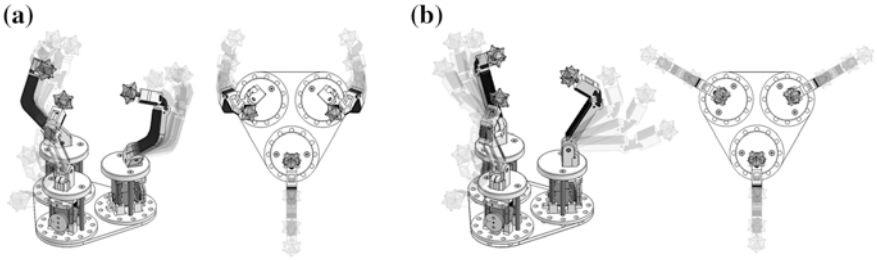

Fig. 3 Overlays that show the difference in finger trajectories between the fingers in the proposed hand (**a**) and those of a traditional hand (**b**)

help accommodate finger reconfigurations during precision manipulation, but has one primary degree of freedom.

As described in Sect. 2 and shown in Fig. 1, the joints for two of the fingers are angled such that their axes of rotation intersect at a common point. The remaining thumb has two linear links. Unlike traditional two-link fingers, the swing trajectories of the curved fingers do not exclusively lie within a plane. A comparison of the differences of this kinematic behavior between the proposed hand and a traditional finger/palm layout is shown in Fig. 3.

Slip at contact is a common issue in precision manipulation, particularly for underactuated hands. The closed-chain model assumes point contacts without slip. To this end, we developed a compliant, rotary fingertip, made of material Vytaflex 40 [26] extending a novel design first proposed in [27] that behaves like a spherical joint when contact is maintained. Different rotary fingertips, as well as active finger surfaces, have been previously proposed in other robotic hand designs [28, 29].

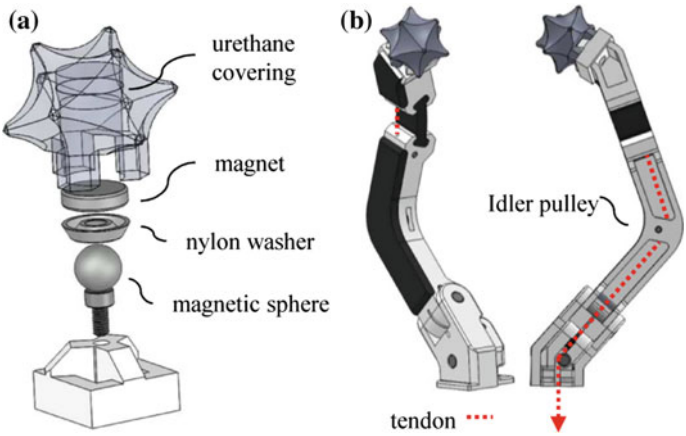

Fig. 4 **a** Components of the rotary fingertip that minimizes slip at contact and **b** views of the curved fingers proposed in this design

The fingertip, shown in Fig. 4, has an icosahedron shape, cast in a rubber urethane with a multi-part mold. In ideal conditions, the icosahedron establishes three points of contact with the grasped object and minimizes slip. The fingertip encapsulates a magnetic spherical joint comprised of a chrome-plated magnetic sphere, a nylon countersunk washer, and a Ø 12.7 mm, N48 neodymium cylindrical magnet. The magnetic components re-center the fingertip when disengaged from the object.

4 Performance

4.1 Test Rig

To evaluate the performance of the proposed hand, a modular test setup utilizing Dynamixel RX-28 servos, pictured in Fig. 1, was built. Each of the three fingers utilized mechanical parameters prevalent in past OpenHand designs [23]: a transmission ratio $(R_{Distal}/R_{Proximal})$ of 1.0 and effective pulley radius 9 mm, a linkage ratio (L_D/L_P) of 0.6, and a joint stiffness ratio (K_D/K_P) of 2.5. Consistent with anthropomorphic proportions, we implemented a $\left(L_{Finger}/L_{Thumb}\right)$ ratio of 1.5 and a base length where $\left(L_{Finger}/L_{Base}\right)$ is approximately 1.25. The angular tilt of the joints in the curved fingers was set according to the base length to produce the common fixed point described in Sect. 2. To simplify fabrication, for the fingertips in particular, the total finger length was 150 mm, approximately 1.5× the length used in commercial hands.

4.2 Manipulation Capabilities

To determine the in-hand manipulation workspace, a triangular object with side length 120 mm was instrumented with an Ascension trakSTAR sensor, which measures position and orientation with resolution 0.5 mm and 0.001 rad, respectively [30]. This object was initialized in a central pinch grasp, and the actuation space was sampled with servo step size 0.1 rad and a corresponding discrete tendon length 1.1 mm. From this initial grasp, we commanded the test setup to move to each point in actuation space and back, and we manually logged whether the object remained in a stable grasp during each operation. We measured the displacement between the initial pinch grasp and the commanded configuration, as well as the displacement error between the initial and final pinch grasps. The measured error provides an indication of how much undesired slip occurred during the motion. The object was released and reset prior to each test. All motions were recorded relative to the initial pinch grasp of each trial, instead of the trakSTAR's global coordinate frame.

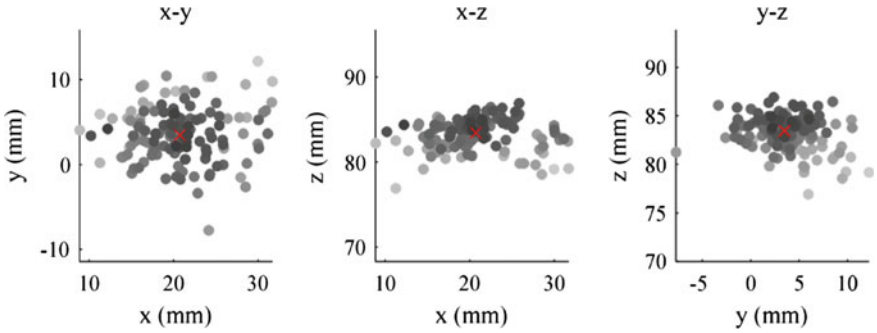

Fig. 5 The measured workspace for the triangular test object grasped by the hand. *Lighter shading* indicates a larger Cartesian motion error between the initial and final pinch grasps

Figure 5 details the characteristics of the measured workspace for the specified test object. The coordinate frame of the workspace is centered at the centroid of the hand base, with the x-axis pointed towards the thumb and the z-axis pointed upwards. The measured Cartesian coordinates were scaled down to account for the increased size of the test rig, making the final results comparable to those previously measured for a traditional finger/palm layout of commercial size [1]. The results show that the $x - y$ projection of the Cartesian workspace is approximately a circle of 18 mm diameter for the points with a measured average error of less than 3.2 mm, the maximum motion in the z direction for such points was approximately 5.1 mm. This small magnitude of vertical displacement is expected since the hand is designed for allowing the grasped object to rotate about a fixed point; this characteristic is conceived to facilitate the reorientation of the grasped body in space, an essential behavior for in-hand manipulation.

While the whole results apparently do not show a significant increase in the overall workspace compared to our prior work [4], the results indeed show that the

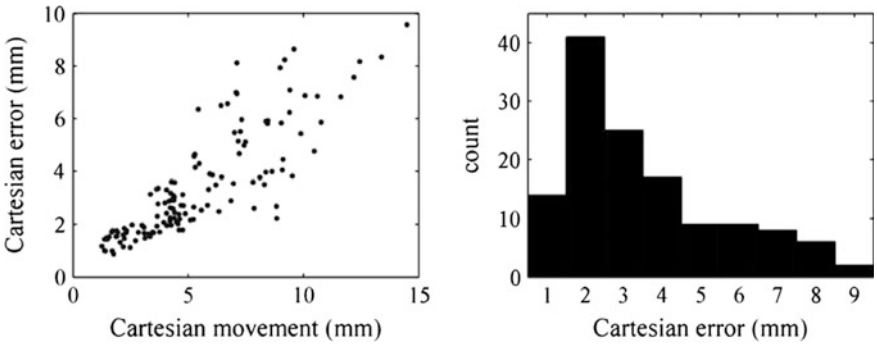

Fig. 6 On the *left*, measured error increases as the magnitude of the commanded motion increases. The measured error, an indication of the amount of slip, was less than 10 mm for all test trials presented in this paper

rotary fingertips reduced the slip at contact and limited 90 % of measured errors in the achievable workspace to be less than 3 mm between the initial and final pinch configurations, as presented in the histogram of Fig. 6.

5 Conclusions and Future Work

In this paper, we proposed and evaluated an underactuated hand that extends the in-hand manipulation capabilities of existing commercial designs with morphological changes inspired by the properties of parallel wrists without significantly reducing the hand's pre-existing power-grasping capabilities. We demonstrated that robotic fingers can be enhanced with rotary fingertips to reduce rolling and slip effects at contact points, making the system behavior more similar to that assumed by the closed-kinematic-chain model of precision manipulation. This work suggests that selecting design parameters for the hand-object system as a whole can result in novel behaviors. Our initial proof-of-concept did not attempt to optimize for non-kinematic parameters in the system, such as the transmission and joint stiffness ratios; studying the reconfiguration of the system under these parameters will be critical in expanding the usable workspace during precision manipulation tasks. Future work will also focus on producing an appropriately-sized hand implemented with the curved fingers suggested in this paper, so that a direct comparison with traditional finger/palm layouts can be made.

References

1. Bullock, I.M., Ma, R.R., Dollar, A.M.: A hand-centric classification of human and robot dexterous manipulation. IEEE Trans. Haptics **6**(2), 129–144 (2013)
2. Ma, R.R., Dollar, A.M.: On dexterity and dexterous manipulation. ICAR (2011)
3. Li, Z., Hsu, P., Sastry, S.: Grasping and coordinate manipulation by a multifingered robot hand. Int. J. Robot. Res. **8**(4), 33–50 (1989)
4. Odhner, L.U., Ma, R.R., Dollar, A.M.: Exploring dexterous manipulation workspaces with the iHY Hand. J. Robot. Soc. Jpn. **32**(4), 318–322 (2014)
5. Balasubramanian, R., Belter, J.T., Dollar, A.M.: Disturbance response of two-link underactuated serial-link chains. J. Mech. Robot. **4**(2) (2012)
6. Birglen, L., Gosselin, C., Laliberté, T.: Underactuated Robotic Hands, vol. 40. Springer, Berlin (2008)
7. Kerr, J., Roth, B.: Analysis of multifingered hands. Int. J. Robot. Res. **4**(4), 3–17 (1986)
8. Bicchi, A., Melchiorri, C., Balluchi, D.: On the mobility and manipulability of general multiple limb robots. IEEE Trans. Robot. Autom. **11**(2), 215–228 (1995)
9. Rojas, N., Dollar, A.M.: Characterization of the precision manipulation capabilities of robot hands via the continuous group of displacements. In: IROS (2014)
10. Borràs, J., Dollar, A.M.: Analyzing dexterous hands using a parallel robots framework. Autonom. Robots **36**(1–2), 169–180 (2014)
11. Ebert-Uphoff, I., Voglewede, P.A.: On the connections between cable-driven robots, parallel manipulators and grasping. In: ICRA (2004)

12. Di Gregorio, R.: Kinematics of the 3-UPU wrist. Mech. Mach. Theory **38**(3), 253–263 (2003)
13. Carricato, M., Parenti-Castelli, V.: A novel fully decoupled two-degrees-of-freedom parallel wrist. Int. J. Robot. Res. **23**(6), 661–667 (2004)
14. Ulrich, N., Paul, R., Bajcsy, R.: A medium-complexity compliant end effector. In: ICRA (1988)
15. Robotiq 3-finger adaptive robot gripper. http://www.robotiq.com/en/products/industrial-robot-hand/
16. Odhner, L.U., Jentoft, L.P., Claffee, M.R., Corson, N., Tenzer, Y., Ma, R.R., Buehler, M., Kohout, R., Howe, R.D., Dollar, A.M.: A compliant, underactuated hand for robust manipulation. Int. J. Robot. Res. **33**(5), 736–752 (2014)
17. Hervé, J.M.: Analyse structurelle des mécanismes par groupe des deplacements. Mech. Mach. Theory **13**(4), 437–450 (1978)
18. Hunt, K.H.: Kinematic Geometry of Mechanisms. Oxford University Press, Clarendon (1978)
19. Tischler, C.R., Samuel, A.E., Hunt, K.H.: Kinematic chains for robot hands-II. Kinematic constraints, classification, connectivity, and actuation. Mech. Mach. Theory **30**, 1217–1239 (1995)
20. Hervé, J.M.: Note about the 3-UPU wrist. Mec. Mach. Theory **39**, 901–904 (2004)
21. Qinchuan, L., Zhen, H., Hervé, J.M.: Type synthesis of 3R2T 5-DOF parallel mechanisms using the Lie group of displacements. IEEE Trans. Robot. Autom. **20**, 173–180 (2004)
22. Fanghella, P., Galletti, C.: Particular or general methods in robot kinematics?: both particular and general. Mech. Mach. Theory **24**, 383–394 (1989)
23. Ma, R.R., Odhner, L.U., Dollar, A.M.: A modular, open-source 3d printed underactuated hand. In: ICRA (2013)
24. Ma, R.R., Belter, J.T., Dollar, A.M.: Hybrid deposition manufacturing: design strategies for multi-material mechanisms via 3D-printing and material deposition. J. Mech. Robot. (2015)
25. Smooth-On PMC®-780 Industrial Urethane Rubber Compound. http://www.smooth-on.com/Urethane-Rubber-an/c6_1117_1148/index.html
26. Smooth-On Vytaflex® Urethane Rubber—For Perfect Concrete Castings. http://www.smooth-on.com/Urethane-Rubber-an/c6_1117_1142/index.html
27. Hunt, K.H., Torfason, L.E.: A three-fingered pantograph manipulator—a kinematic study. J. Mech. Des. **109**(2), 171–177 (1987)
28. Bicchi, A., Marigo, A.: Dexterous grippers: putting nonholonomy to work for fine manipulation. Int. J. Robot. Res. **21**(5–6), 427–442 (2002)
29. Tincani, V., Catalano, M.G., Farnioli, E., Garabini, M., Grioli, G., Fantoni, G., Bicchi, A.: Velvet fingers: a dexterous gripper with active surfaces. In: IROS, pp. 1257–1263 (2012)
30. Ascension Technology Corporation. http://www.ascension-tech.com/medical/pdf/TrakStarWRTSpecSheet.pdf